



# HHS Public Access

Author manuscript

Biochemistry. Author manuscript; available in PMC 2017 February 16.

Published in final edited form as:

*Biochemistry*. 2016 February 16; 55(6): 960–969. doi:10.1021/acs.biochem.5b01157.

## Intramolecular Cleavage of the hASRGL1 Homodimer Occurs in Two Stages

Wenzong Li<sup>†</sup>, Seema Irani<sup>‡</sup>, Amanda Crutchfield<sup>†</sup>, Kristal Hodge<sup>†</sup>, Wendy Matthews<sup>†</sup>, Pooja Patel<sup>†</sup>, Yan Jessie Zhang<sup>\*,†,§</sup>, and Everett Stone<sup>\*,†</sup>

<sup>†</sup>Department of Molecular Biosciences, University of Texas, Austin, Texas 78712, United States

<sup>‡</sup>Department of Chemical Engineering, University of Texas, Austin, Texas 78712, United States

<sup>§</sup>Institute of Cellular and Molecular Biology, University of Texas, Austin, Texas 78712, United States

### Abstract

The human asparaginase-like protein 1 (hASRGL1) is a member of the N-terminal nucleophile (Ntn) family that hydrolyzes L-asparagine and isoaspartyl-dipeptides. The nascent protein folds into an  $\alpha\beta$ - $\beta\alpha$  sandwich fold homodimer that cleaves its own peptide backbone at the G167–T168 bond, resulting in the active form of the enzyme. However, biophysical studies of hASRGL1 are difficult because of the curious fact that intramolecular cleavage of the G167–T168 peptide bond reaches only 50% completion. We capitalized upon our previous observation that intramolecular processing increases thermostability and developed a differential scanning fluorimetry assay that allowed direct detection of distinct processing intermediates for the first time. A kinetic analysis of these intermediates revealed that cleavage of one subunit of the hASRGL1 subunit drastically reduces the processing rate of the adjacent monomer, and a mutagenesis study showed that stabilization of the dimer interface plays a critical role in this process. We also report a comprehensive analysis of conserved active site residues and delineate their relative roles in autoprocesing and substrate hydrolysis. In addition to glycine, which was previously reported to selectively accelerate hASRGL1 cleavage, we identified several novel small molecule activators that also promote intramolecular processing. The structure–activity analysis supports the hypothesis that multiple negatively charged small molecules interact within the active site of hASRGL1 to act as a base in promoting cleavage. Overall, our investigation provides a mechanistic understanding of the maturation process of this Ntn hydrolase family member.

\*Corresponding Authors: Address: 1 University Station A5300, Austin, TX 78712. jzhang@cm.utexas.edu. Phone: (512) 471-8645. Fax: (512) 471-9469. Address: 1 University Station C0800, Austin, TX 78712. stonesci@utexas.edu. Phone: (512) 232-4103.

**Accession Codes**  
PDB entry 4ZM9.

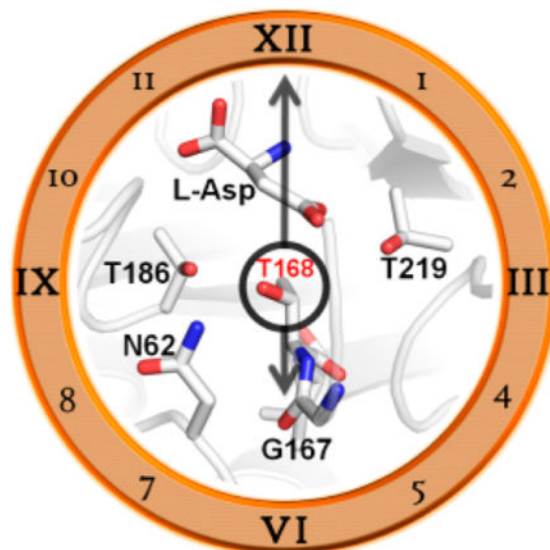
### Notes

The authors declare no competing financial interest.

### Supporting Information

The Supporting Information is available free of charge on the ACS Publications website at DOI: 10.1021/acs.bio-chem.5b01157. SDS–PAGE analysis of wt-hASRGL1 incubated with 1 M glycine over time (Figure S1), SEC chromatograms of wt-hASRGL1 and hASRGL1-C202 variants (Figure S2), composite SDS–PAGE gel of wt-hASRGL1 and hASRGL1-C202 variants (Figure S3), thermal transition temperatures of wt-hASRGL1 and hASRGL1 variants (Table S1), and thermal transition temperatures of hASRGL1 activated with small molecules (Table S2) (PDF)

## Graphical abstract



The human asparaginase-like protein 1 (hASRGL1) (EC 3.4.19.5) catalyzes the hydrolysis of L-asparagine and isoaspartyl-dipeptides.<sup>1</sup> As a member of the N-terminal nucleophile (Ntn) hydrolase family, hASRGL1 is translated as a polypeptide precursor that forms an  $\alpha\beta$ - $\beta\alpha$  sandwich fold homodimer that subsequently undergoes an intramolecular cleavage to create the active form of the enzyme. The side chain of an active site  $\beta$ -subunit threonine (Thr168) is believed to be the critical nucleophile that catalyzes intramolecular processing. During this activation step, an acyl shift reaction occurs with the hydroxyl group of Thr168 attacking the carbonyl group of the preceding amino acid and forming an ester intermediate that is subsequently hydrolyzed to expose the N-terminal residue of the nascent  $\beta$ -subunit.<sup>1</sup> Once hASRGL1 is activated, its biological function is thought to be the clearing of isoaspartate-containing peptides that accumulate as a common source of nonenzymatic protein damage under physiological conditions.<sup>2</sup> Furthermore, the hASRGL1 asparaginase activity has generated interest in the therapeutic development of hASRGL1 as a potentially nonimmunogenic alternative to the bacterial asparaginases used to clinically treat acute lymphoblastic leukemia.<sup>3</sup>

*In vitro* studies of hASRGL1 are difficult as intramolecular processing of purified recombinant hASRGL1 is slow and has the puzzling phenomenon of achieving up to only 50% cleavage. This partial activation results in a mixture of active and inactive protein that greatly hinders characterization of the biophysical properties of the enzyme. However, several methods for obtaining completely processed enzyme that facilitate the quantification of kinetic properties of the enzyme and structural study have recently been reported. One method yielding fully active enzyme involves the bicistronic co-expression of the separate  $\alpha$  and  $\beta$  subunits, with the main disadvantage being very low yields of properly assembled protein.<sup>4</sup> The finding that free glycine (Gly) accelerates and facilitates full intramolecular cleavage of wt-hASRGL1 was another significant advance,<sup>5</sup> although mutational studies of active site residues have shown that glycine does not always facilitate autoprocesing,

rendering kinetic quantitation difficult or impossible in certain cases.<sup>3</sup> Our group also previously solved this issue by creating a fully activated version of hASRGL1 by means of a circular permutation (cp-hASRGL1). This engineering design physically links the original N- and C-termini, and the protein is now expressed such that the active site nucleophile Thr168 is the new N-terminus once the initiator Met residue is cleaved during translation.<sup>6</sup> The cp-hASRGL1 construct therefore uncouples the intramolecular processing event needed for subsequent hydrolysis of substrate. The utility of this approach is evidenced by high expression yields and enzymatic activity that is comparable to that of fully activated wt-hASRGL1. This strategy allows the characterization of active site variants such as hASRGL1-Thr168Ser that are incapable of intramolecular processing (even in the presence of high glycine concentrations).<sup>3,6</sup>

Our prior analyses revealed that the nucleophilic residue Thr168 imparts a large steric strain within the active site that is relaxed after the cleavage event and thermally stabilizes hASRGL1.<sup>6</sup> In this study, we exploited this property of the enzyme and developed a differential scanning fluorimetry (DSF) assay that can quantify individual hASRGL1 species formed during activation. This advance allowed observation for the first time of three distinct molecular complexes during maturation, namely, the unprocessed  $\alpha\beta\text{-}\beta\alpha$  homodimer, a half-processed  $\alpha\beta\text{-}\beta\alpha$  heterotrimer, and the fully processed  $\alpha\beta\text{-}\beta\alpha$  heterotetramer. Intriguingly, this method revealed that the rate of cleavage of the first  $\alpha\beta$  subunit is significantly faster than the rate of the second cleavage event. These large rate differences explain why recombinant hASRGL1 proceeds only to the half-processed  $\alpha\beta\text{-}\beta\alpha$  heterotrimer species. A subsequent mutagenesis experiment showed that the dimer-dimer interface is critical for intramolecular processing. We also used both the wt-hASRGL1 and cp-hASRGL1 scaffolds as platforms for delineating the roles of highly conserved active site residues in catalyzing intramolecular processing and/or substrate hydrolysis. Additionally, biochemical studies that identified additional small molecules (besides glycine) that can accelerate hASRGL1 processing were undertaken, pinpointing the importance of critical contacts in the active site between the activator and protein.

## EXPERIMENTAL PROCEDURES

### Materials

Oligonucleotides were purchased from Integrated DNA Technologies (Coralville, IA). Phusion DNA Polymerase and dNTPs were from New England Biolabs (Ipswich, MA). Crystal Screening Kits were from Hampton Research (Aliso Viejo, CA). All other reagents were from Sigma-Aldrich unless otherwise mentioned.

### Cloning, Expression, and Purification of hASRGL1 and Variants

The construction of hASRGL1 and circularly permuted hASRGL1 (cp-hASRGL1) has been described previously.<sup>1,6</sup> The hASRGL1/cp-hASRGL1 point mutations were generated using the QuikChange Site Directed Muta-genesis Kit (Stratagene). All genes were cloned into a pET28a vector and sequenced to verify there were no undesired mutations. The recombinant expression and purification of proteins was performed as previously described.<sup>6</sup> Briefly, cultures of *Escherichia coli* (DE3) cells expressing hASRGL1 or variants were

induced upon reaching an OD<sub>600</sub> of 0.8 with 500  $\mu$ M (final concentration) isopropyl  $\beta$ -D-1-thiogalactopyranoside (IPTG) and allowed to express protein for 12 h at 16 °C. After the expression cultures had been harvested by centrifugation, the pellet was resuspended and lysed by sonication. After clarification, the enzymes were purified using a Ni<sup>2+</sup>-NTA affinity column, followed by a chromatography step using a monoQ ion exchange column (GE Healthcare). The proteins were then polished by gel filtration chromatography. The purified proteins were concentrated to ~10 mg/mL and flash-frozen with liquid nitrogen before being stored at -80 °C.

### **T<sub>M</sub> Measurements using Differential Scanning Fluorometry**

Purified hASRGL1 variants were diluted to ~1 mg/mL in buffer containing 50 mM HEPES (pH 7.5) and 100 mM NaCl. Protein variants were dispensed into 96-well low-profile polymerase chain reaction (PCR) plates (ABgene, Thermo Scientific) at a volume of 18  $\mu$ L in each well. 10 $\times$  SYPRO Orange (Molecular Probes, Invitrogen) was added to each well, and the contents were mixed well prior to centrifugation. Plates were sealed with adhesive heat seals (ABgene, Thermo Scientific) to prevent evaporation. The DSF thermal shift assay was conducted using a LightCycler 480 RT-PCR instrument (Roche). The experiments were conducted with a continuous temperature acquisition mode of 10 acquisitions/°C in each cycle from 20 to 95 °C. T<sub>M</sub> values from the resulting data were derived using the Boltzmann equation.<sup>7</sup>

### **Small Molecule Activation Assay**

The wt-hASRGL1 enzyme (~1 mg/mL) was incubated with 1 M glycine at 37 °C for 48 h in a buffer containing 50 mM HEPES, 100 mM NaCl, and 10 mM  $\beta$ -mercaptoethanol (pH 7.5). Aliquots were taken at various time points for DSF assays and sodium dodecyl sulfate–polyacrylamide gel electrophoresis (SDS–PAGE) gel density analyses. Differential scanning fluorimetry data were analyzed using Magic Plot software (Magic Plot System, LLC) by taking the derivative of each melting curve followed by summation of Gaussian equations to determine the T<sub>M</sub> and the area of each peak to calculate the fraction of each species observed during autoprocesing. The resulting areas were then fitted to a kinetic model (Figure 1) using KinTek software (KinTek Corp.) to obtain intramolecular processing rates.

For the study of small molecule activators, wt-hASRGL1 protein was diluted to a final concentration at 1 mg/mL for each processing reaction. Solutions of ammonium carbamate, ammonium chloride, ammonium citrate, ammonium phosphate, ammonium sulfate,  $\beta$ -alanine, betaine (*N*-trimethylglycine), glycine methyl ester, glycinamide, sarcosine, and sodium bicarbonate were added to final concentrations of 1, 0.5, and 0.25 M; *o*-phosphorylethanolamine was added at final concentrations of 0.9, 0.5, and 0.25 M, and taurine was added at final concentrations of 0.225, 0.1, and 0.05 M. The mixtures were incubated at 37 °C for 48 h. Aliquots were taken at various time points for DSF assays and SDS–PAGE gel density analyses. The SDS–PAGE band intensities were quantified by Image Lab (Bio-Rad). Percentages were calculated on the basis of uncleaved band intensity relative to the sum of all forms (uncleaved + cleaved). Kinetic characterization of the autoprocesing of hASRGL1 variants was performed as described for the wt-hASRGL1 enzyme.

## Crystallization

The cp-hASRGL1 enzyme was concentrated to approximately 10 mg/mL in a buffer containing 20 mM HEPES (pH 7.5), 50 mM NaCl, and 10 mM  $\beta$ -mercaptoethanol. Sparse-matrix crystal screening was performed using a Phoenix liquid handling system (Art Robbins Instruments). After the identification of initial hits, crystallization conditions were optimized by mixing 1  $\mu$ L of pretreated cp-hASRGL1 or variants with 1  $\mu$ L of a crystallization solution in a matrix of 22–25% PEG4000, 4 mM DTT, and 0.15 mM sodium citrate (pH 4.6). Microseeding was utilized to generate larger crystals. Needle-like crystals were observed within 3 days. To obtain the complex structure of cp-hASRGL1 and glycine, protein was incubated with 50 mM glycine for 3 h on ice prior to crystal tray setup. A cryoprotectant solution [30% glycerol (v/v) in a crystallization solution] was applied to the crystals prior to vitrification in liquid nitrogen in preparation for data collection.

## Diffraction Data Collection and Structure Determination

X-ray diffraction data of the cp-hASRGL1–glycine complex were collected from synchrotron radiation at beamline 5.0.3 at the Advanced Light Source (Berkeley, CA). The resulting data were processed and scaled using the HKL2000 software suite.<sup>8</sup> Data collection statistics are listed in Table 1.

The structure of cp-hASRGL1 complexed with glycine was determined using molecular replacement by Phaser-MR from the Phenix suite<sup>9</sup> with our previously published hASRGL1 T168A structure [Protein Data Bank (PDB) entry 3TKJ] as a search model.<sup>6</sup> Structures were refined with phenix.refine<sup>9</sup> along with iterative model building in COOT.<sup>10</sup> Noncrystallographic symmetry (NCS restraints) and TLS parameters were applied in the refinements. In the refinement, 5% of the test set was excluded for  $R_{\text{free}}$  cross-validation.<sup>11</sup> The final model was evaluated by PROCHECK<sup>12</sup> and MolProbity.<sup>13</sup> Refinement statistics are listed in Table 1.

## L-Aspartic acid $\beta$ -hydroxamate (AHA activity assay)

Reactions of hASRGL1 or hASRGL1 variants with AHA were conducted in a buffer containing 50 mM HEPES (pH 7.5) and 100 mM NaCl at 37 °C. Most enzyme/substrate mixtures were assayed using 0.3  $\mu$ M enzyme (final concentration) and allowed to react for 20 s. The hASRGL1 variants were allowed to react for longer times depending on their activity (20–600 s). The reactions, each with a total volume of 100  $\mu$ L, were quenched with 10  $\mu$ L of 12% (w/v) trichloroacetic acid (TCA). Subsequently, 50  $\mu$ L of color reagent (1:3 ratio of 2% 8-hydroxyquinoline in ethanol to 1 M Na<sub>2</sub>CO<sub>3</sub>) was mixed with the reaction solution, heated to 100 °C for 4 min, and then cooled to 4 °C for 10 min for color development. The formation of hydroxylamine product was quantified by measuring the absorbance of the product at 705 nm on a Tecan infinite 200 instrument (Tecan Group Ltd.). Product concentrations were assessed by construction of a hydroxylamine standard curve under the same conditions. All reactions were repeated in triplicate, and the observed rates were fitted to the Michaelis–Menten equation using Kaleidagraph 4.5.2 (Synergy).

## Construction and Screening of a hASRGL1-C201A Error-Prone Library

A library based on the coding sequence of hASRGL1-C201A was generated by error-prone PCR with 0.4 ng/ $\mu$ L template and 0.5  $\mu$ M primers [forward primer (5'-ATAACAATTCCCCTCTAGAAATAATTTT) and reverse primer (5'-TTGTCTACGGAGCTCGAATTCTC)]. The concentrations of dNTPs used were 0.23 mM for dATP, 0.2 mM for dCTP, 0.57 mM for dGTP, and 4 mM for dTTP. The PCR was performed using *Taq* DNA polymerase (New England Biolabs). The gene products were subsequently cloned into expression vector pET28a.

The resulting library plasmids were subsequently transformed into *E. coli* strain BL21(DE3) [ *ansA*, *ansB*, *iaaA*] containing deletions of the three native asparaginases used for library screening. Cells were grown in nonselective LB medium overnight, at which point approximately  $10^9$  cells were transferred to 25 mL of fresh LB culture and grown to an OD<sub>600</sub> of 2.0. One milliliter of culture was collected by centrifugation and resuspended in 1 mL of selective medium (1  $\times$  M9 medium supplemented with 0.4% glucose, 0.1  $\mu$ g/mL thiamine, 1 mM MgSO<sub>4</sub>, 0.1 mM CaCl<sub>2</sub>, 0.01 mM FeSO<sub>4</sub>, 5 mM Asn, 50  $\mu$ g/mL kanamycin, and IPTG) and plated on selective medium plates. Colonies started appearing after incubation at 37 °C for 3 days, and those with significantly greater size were selected for sequencing.

## RESULTS AND DISCUSSION

### The First hASRGL1 Intramolecular Cleavage Step Is Significantly Faster Than the Second

wt-hASRGL1 undergoes intramolecular processing at a rate of  $\sim 0.034 \text{ h}^{-16}$  and, as assessed by gel densitometry, rarely proceeds beyond  $\sim 50\%$  cleavage. There are two possibilities for the identity of this pool of 50% processed protein: a mixture of an equal amount of unprocessed dimer and cleaved  $\alpha/\beta-\beta/\alpha$  heterotetramer or an accumulation of half-processed  $\alpha/\beta-\beta\alpha$  heterotrimer (Figure 1). However, SDS-PAGE detects only the total amount of cleaved and uncleaved species, whereas intermediate species cannot be distinguished in the gel. To this end, we exploited our previous observation that the activation process of hASRGL1 improves thermal stability.<sup>6</sup> Indeed, the unprocessed wt-hASRGL1 exhibits a  $T_M$  of 61 °C, while the hASRGL-T168A and -S variants or the fully active cp-hASRGL1 is much more stable with a  $T_M$  of  $\sim 70$  °C. The T168  $\gamma$ -methyl group imparts steric strain in the nascent enzyme, a strain that is relieved by intramolecular cleavage upon activation. Removal of the  $\gamma$ -methyl group via mutation to the processing incompetent T168A and -S variants and circular permutation to remove the scissile peptide bond both avoid this strain and showed a higher stability.<sup>6</sup> We reasoned that measuring hASRGL1 thermostability as a function of time during activation might be a means of distinguishing between different molecular species that accumulate in solution. The predicted outcome would thus be one initial (unprocessed) peak at a  $T_M$  of  $\sim 60$  °C that partially resolves into a peak at a  $T_M$  of  $\sim 70$  °C, consistent with fully activated hASRGL1. However, after incubation for 48 h, instead of two distinctive peaks (corresponding to unprocessed and processed), we observed a single new peak at a  $T_M$  of  $\sim 65$  °C. An SDS-PAGE gel was run to establish the identity of the protein with a  $T_M$  of 65 °C, and as previously observed and reported, we found three bands wherein 50% of the sample is a 33 kDa species corresponding to uncut protein and

50% of the sample is comprised of 18 and 15 kDa species that correspond to the  $\alpha$  and  $\beta$  subunits of hASRGL1 after processing.<sup>1,5</sup> We noted that the  $dF/dT$  (change in fluorescence/change in temperature) curves from this experiment were asymmetrical in appearance; thus, to gain further insight, we fit the area under the  $dF/dT$  curves by summation of multiple Gaussian equations (MagicPlot Student, Magicplot Systems LLC). As shown in Figure 2A, at time 0 h, the  $dF/dT$  area is well fitted to three Gaussian curves with the main peak at 61 °C and two shoulders at 56 and 65 °C. At the 8 h time point (Figure 2B), the 65 °C peak is now the major species, and by 48 h, the 61 °C peak is gone with the appearance of a small new shoulder at ~71 °C (Figure 2C). We speculated that the identity of the peaks at 61, 65, and 71 °C might represent uncleaved, intermediate, and a small fraction of fully cleaved  $\alpha/\beta-\beta/\alpha$  heterotetramer, respectively. The shoulder at 56 °C did not appear to change over time and likely represents either impurities or misfolded protein. We also note that different preparations of protein after purification have varying levels of processed enzyme at the recorded initiation time.

To test this hypothesis, we repeated the experiment in the presence of 1 M glycine to drive the self-cleavage reaction to completion. We observed that Gly not only accelerated intramolecular processing but also acted as a stabilizing ligand that increased  $T_M$  values for all three species. This allowed clear observation over time of an initial distinct peak at a  $T_M$  of 71 °C that decayed into the transient buildup of an intermediate peak at a  $T_M$  of 79 °C that in turn decayed into a single peak at a  $T_M$  of 86 °C (Figure 3A). SDS-PAGE analyses of the same time points corresponding to the DSF experiments show that the  $T_M = 71$  °C peak is the unprocessed protein, the  $T_M = 86$  °C species is the fully activated tetramer, and solutions containing the intermediate  $T_M = 79$  °C species are a mixture of cleaved and uncleaved protein (Figure S1). Finding that the data are consistent with an intermediate species during activation, we quantified the glycine-promoted processing reaction by fitting the  $dF/dT$  curves to Gaussian equations to obtain peak areas as a function of time. This resulted in data that we fit (using Kintek Explorer Pro, Kintek Corp.) to a simple  $MM \rightarrow MD \rightarrow DD$  two-step cleavage model, wherein  $MM$  represents the unprocessed homodimer,  $MD$  is the half-processed heterotrimer, and  $DD$  is the fully processed heterotetramer (Figure 1). The data were well fit to this model and revealed that the first intramolecular cleavage ( $MM \rightarrow MD$ ) occurs at a rate of  $k_1 = 1 \text{ h}^{-1}$  followed by a slower second cleavage ( $MD \rightarrow DD$ ) at a rate of  $k_2 = 0.4 \text{ h}^{-1}$  (Figure 3B and Table 2). Taken together, these results suggest that in the absence of a small molecule activator like glycine, it is the large difference in rates between the first and second cleavages ( $k_1 = 0.034 \text{ h}^{-1}$ , and est.  $k_2 = 0.002 \text{ h}^{-1}$ ) that explains why intramolecular processing of wt-hASRGL1 proceeds to only ~50% and that the accumulated species is the half-processed  $\alpha/\beta-\beta/\alpha$  heterotrimer. To the best of our knowledge, this is the first direct experimental evidence of an  $\alpha/\beta-\beta/\alpha$  heterotrimer intermediate during autoprocesing.

### Dimer Interface Stabilization Contributes to Intra-molecular Processing

The difference in the hASRGL1 first-and second-subunit hydrolysis rates suggests that the intra-molecular processing of one  $\alpha\beta$  subunit elicits a change to the other subunit such that cleavage is now impaired. Torsional strain is a known driver of processing of hASRGL1, which in light of the data presented here indicates that the first cleavage not only thermally

stabilizes the heterotrimer complex but also may partially relieve the strain in the adjacent uncleaved subunit. It has been observed in other Ntn family members that dimer stabilization/formation is critical for self-cleavage.<sup>14</sup> Thus, we hypothesized that the first cleavage results in a subtle allosteric rearrangement across the dimer–dimer interface that either reduces torsional strain or shifts the conformational equilibrium of the unprocessed active site away from a cleavable state.

To test the idea that the interactions across the dimer interface regulate intramolecular processing, we constructed two interface variants, C202A and C202S, based upon the location of the C202 residue from one subunit being symmetrically adjacent to the C202 residue on the partner protomer. Even though no disulfide bond is formed between the cysteine residues, the configurations of the two thiol side chains form favorable van der Waals interactions. Both variants were designed to weaken the dimer interface between the two molecules by creating a hole in the hydrophobic dimer interface (C202A) or by introduction of a hydrophilic pair (C202S) within a hydrophobic patch. The C202A and C202S variants were both found to express well, and as hypothesized, they exhibited lower  $T_M$  values of approximately 49 °C each (60 °C for wt). Even though the dimer interface is presumably weakened, the formation of dimer was not abolished. The variants formed dimers with a profile similar to that of wt as assessed by size exclusion chromatography (Figure S2), but intramolecular processing was fully inhibited in the absence of glycine in both variants (Figure S3). However, we observed that by using high concentrations of glycine, both C202A and C202S can undergo processing and mature into active proteins. We assessed the glycine-promoted (1 M) cleavage kinetics of these variants and found that C202A had a  $k_1$  of 0.8 h<sup>-1</sup> and a  $k_2$  of 0.3 h<sup>-1</sup> and that C202S was more impaired with a  $k_1$  of 0.6 h<sup>-1</sup> and a  $k_2$  of 0.2 h<sup>-1</sup> (Table 2). Both variants show a reduction in the level of glycine-promoted activation compared to that of the wild type (1 and 0.4 h<sup>-1</sup> for  $k_1$  and  $k_2$ , respectively). These results indicate that the dimer–dimer interface does indeed play a role in both stability and self-cleavage capacity.

In a further effort to determine if compensatory mutations could be found, we used the C202A variant as a starting point to construct an error-prone library that was ultimately transformed into an *E. coli* strain devoid of native asparaginases. Cells expressing this library were spread on minimal medium plates containing L-Asn as the sole nitrogen source such that only hASRGL1-C202A variants that could undergo intra-molecular processing would be able to convert L-Asn to ammonia and allow colony growth. This work led to the isolation of a C202A → A202V variant that restored unliganded thermostability ( $T_M = 59$  °C) and rescued partial intra-molecular processing without glycine ( $k_1 \sim 0.07$  h<sup>-1</sup>). In the presence of glycine, this variant displayed rates similar to that of wt-hASRGL1 with a first-subunit intramolecular cleavage kinetics of  $k_1 = 1.1$  h<sup>-1</sup> and a second-subunit cleavage of  $k_2 = 0.6$  h<sup>-1</sup> (Table 2). Interestingly, once all the variants had been activated, they were shown to have identical steady state kinetic values for substrate hydrolysis. This suggests that although activation and enzymatic activity are interrelated, they are actually governed differently in this family of proteins.

In summary, our data suggest that dimer interface formation is critical for allowing one of the hASRGL1 subunits to undergo intramolecular processing. One apparent commonality to



the NTN family of hydrolases is the necessity of forming a strained or “twisted” conformation at the scissile peptide bond<sup>14–16</sup> such that the nucleophile is close enough to attack the carbonyl group of the preceding amino acid. The fact that each subsequent cleavage event of hASRGL1 (and variants) results in a similar increase in  $T_M$  [8–9 °C with glycine for either MM → MD or MD → DD (Table S1)] suggests that torsional restraint from the T168 side chain<sup>6</sup> is independently maintained and is not relaxed in the unprocessed subunit upon cleavage of the other protomer. Thus, we propose that the substantially slower second-subunit cleavage rate (MD → DD) is an indication that the equilibrium describing the scissile peptide bond (G167–T168) has shifted away from a strained conformation. As dimer–dimer stabilization/interactions appear to play a significant role in achieving this scissile bond strain, this suggests that hydrolysis of one protomer and the resulting increase in entropy after forming the  $\alpha/\beta$ - $\beta/\alpha$  heterotrimer decreases the probability of creating the strained configuration.

### Studies of the Role of Conserved Active Site Residues in Substrate Catalysis and Intramolecular Processing

Inspection of hASRGL1 structures shows that the relative locations of the two amide hydrolysis reactions that the nucleophilic T168 residue must facilitate, namely, the G167–T168 peptide bond and the substrate amide bond, are roughly positioned at 6 and 12 o'clock from each other (Figure 4A). In this same overly simplified manner, the highly conserved active site residues N62, T186, and T219 are oriented in an ~8, 10, and 2 o'clock pattern, respectively, all within ~4 Å of nucleophile T168. The positions of N62, T186, and T219 relative to the location of the substrate and the G167–T168 peptide bond led us to hypothesize that these active site residues may play differing roles in promoting intramolecular processing as well as substrate hydrolysis. Similarly, a previous study of hASRGL1 showed that T219 and T186 provide an essential hydrogen bond network that facilitates both intra-molecular processing and substrate catalysis where it was reported that T219V, T219A, and T186V variants required large amounts of glycine to achieve (partial) cleavage but displayed no detectable L-Asn hydrolysis.<sup>3</sup> We initiated a mutagenesis study by constructing N62D/A, T186A/S, and T219A/S active site variants to assess their role in substrate catalysis as well as processing. Using the cp-hASRGL1 platform as a way to obtain fully activated enzyme along with the use of the asparaginase substrate analogue, L-aspartic acid  $\beta$ -hydroxamate (AHA) provided an ideal way to detect activity of these mutated variants.<sup>6</sup> Hydrolysis of AHA yields not only L-Asp but also hydroxylamine, which is easily detected.<sup>17</sup> We note that the leaving groups of both L-Asn and AHA will require protonation during hydrolysis, but their respective  $pK_a$  values differ greatly (i.e.,  $\text{NH}_4^+ \leftrightarrow \text{NH}_3$ ,  $pK_a = 9.25$ ;  $\text{NH}_3^+-\text{OH} \leftrightarrow \text{NH}_2-\text{OH}$ ,  $pK_a = 5.96$ <sup>18</sup>). Thus, at physiological pH values, hydroxylamine is a stable leaving group and unlike ammonia does not require an extra protonation step. The same mutations were also generated in the native gene format to quantitatively assess their ability to undergo intramolecular processing using our DSF assay.

All constructs described above were well expressed, and SDS–PAGE analysis of the purified, natively expressed variants showed that after incubation for 48 h in the absence of glycine the T219A, T219S, and T186S enzymes showed evidence of ~50% cleavage similar to that of wt-hASRGL1 controls. In contrast, the N62D variant was 5–10% activated while

the N62A and T186A variants showed no observable autoprocessing. The addition of 50 mM glycine facilitated cleavage in all cases, but only wt-hASRGL1, T219A, T219S, and T186S were found to be nearly completely activated by 48 h. A higher concentration of glycine (1 M) promoted the maturation of all variants to completion except for the hASRGL1 T186A, N62D, N62A variants, which were only 85, 70, and 34% processed, respectively, as observed on the gel. To quantify the process of glycine-promoted activation, we measured  $T_M$  values as a function of time by the DSF assay (up to 48 h). Not surprisingly, and as shown in Table 2, all variants displayed a decreased rate of glycine-promoted intramolecular processing compared to that of wt-hASRGL1, ranging from 2- to 20-fold lower (for  $k_1$  or  $k_2$ ) (see Table 2). In particular, a  $T_M$  analysis of hASRGL1-N62A showed only one shift in thermostability, suggesting that the N62A variant is incapable of forming the fully processed  $\alpha\beta\beta'a$  heterotetramer by itself or with a low concentration of glycine, consistent with our observation by SDS-PAGE. This processing defect is partially rescued by a high glycine concentration. Our studies pinpoint that N62 and to a lesser extent T186 are essential for both the autoprocessing and glycine-promoted activation of hASRGL1.

To investigate the role of these residues in substrate catalysis, we expressed and purified these variants in the circularly permuted format and measured their steady state kinetic parameters toward the hydrolysis of AHA. All variants were able to utilize AHA as a substrate, and we observed that the N62D and -A substitutions and the conservative T186S and T219S mutations caused a decrease in catalytic activity,  $k_{cat}$  values ranging from 2- to 26-fold lower compared to that of wt-hASRGL1 (see Table 3). However, the T219A and T186A mutations caused 100- and 530-fold decreases in  $k_{cat}$ , respectively, compared to that of the wt enzyme, strikingly large changes compared to the change in their glycine-promoted cleavage kinetics.

Taking all the processing and substrate kinetic data of the N62, T186, and T219 variants together in the context of their location relative to the substrate and the T186-G167 peptide bond reaction centers allows several postulates to be proposed (Figure 4A). First, cleavage of the T168-G167 peptide bond (6 o'clock) is initiated by nucleophilic attack of the T168  $\gamma$ -hydroxyl group that in the absence of glycine absolutely requires the hydrogen bond network provided by N62 and T186 (8 and 10 o'clock, respectively). Structurally, the hydrogen bonds provided by N62 and T186 are well positioned to stabilize and assist in deprotonation of the T168  $\gamma$ -hydroxyl group during attack (Figure 4A,B). Second, T219 (2 o'clock) is more than 6 Å from the T168-G167 peptide bond and is not required for intramolecular processing. Third, after cleavage, the amide group of substrate binds at ~12 o'clock with the (10 o'clock)  $\gamma$ -hydroxyl of T186 again being well positioned and necessary for stabilizing and assisting in deprotonation of the T168  $\gamma$ -hydroxyl group during nucleophilic attack on the substrate amide group. Fourth, the T219  $\gamma$ -hydroxyl at 2 o'clock is <3 Å from the substrate amide group, where it is ideally located to stabilize the Michaelis complex and the transition state (Figure 4A,C). T219 is also likely very important for stabilizing the ammonia leaving group of L-Asn but is not strictly required for the more stable hydroxylamine leaving group from AHA hydrolysis. Fifth, N62 at 8 o'clock is far from the substrate hydrolysis reaction center and only mildly enhances catalytic activity. In

summary, T186 is the key modulator of T168 nucleophilicity for all reactions, N62 is primarily required for intramolecular processing, and T219 is required for robust substrate hydrolysis but not intramolecular processing.

### Screening of Small Molecule Activators of hASRGL1 Intramolecular Processing

Incubation of hASRGL1 with glycine acts to accelerate intramolecular processing by 30-fold for the first subunit cleavage and by ~200-fold for the second subunit cleavage. Previously, it was reported that only glycine appeared to be able to accomplish this rate acceleration, whereas incubation (at 50 mM) of similar small molecules such as glycolic acid, sarcosine (*N*-methyl-glycine), glyoxylic acid, oxalate, choline, ethanolamine, and glycylglycine had no effect at all.<sup>5</sup> To investigate this captivating phenomenon in more depth, we also initiated a screen of potential small molecule activators but used much higher concentrations (0.25–1 M) to help ensure that any potentially weak but positive interactions would be observed. We incubated hASRGL1 for 48 h with ammonium carbamate, ammonium chloride, ammonium citrate, ammonium phosphate, ammonium sulfate,  $\beta$ -alanine, betaine (*N*-trimethyl-glycine), *O*-phosphorylethanolamine, glycine methyl ester, glycinamide, sarcosine, sodium bicarbonate, and taurine. An SDS–PAGE analysis revealed that nearly all hASRGL1 was cleaved in the presence of ammonium carbamate, ammonium phosphate, and sarcosine with the remainder of the molecules having no effect (see Table 4). We then examined the thermal shifts of sarcosine- and ammonium phosphate-promoted cleavage as a function of time by the DSF assay and found  $k_1$  and  $k_2$  values of 0.11 and 0.08 h<sup>-1</sup> for sarcosine and  $k_1$  and  $k_2$  values of 0.06 and 0.04 h<sup>-1</sup> for phosphate, respectively. Sarcosine and ammonium phosphate elicit rates much slower than those measured with glycine but still follow the general trend of the first subunit cleavage occurring at a rate greater than that of the second cleavage ( $k_1 > k_2$ ).

We also noted that hASRGL1 in the presence of sarcosine and phosphate displayed a 6–8 °C decrease in thermal stabilization as compared to hASRGL1 incubated with the same concentration of glycine (Table S2). A clue about this reduced thermostability was revealed by analysis of our crystal structure of cp-hASRGL1 in complex with a glycine molecule. A close inspection shows that glycine is anchored by a salt bridge between its carboxyl group and the side chain of R196; additionally, the Gly amino group has an electrostatic interaction with D199, along with hydrogen bonds to the side chains of S200 and T168 and the carbonyl of G220 (Figure 5). Structurally, the Gly amino group interactions are likely disrupted by even the presence of a single *N*-terminal methyl group (as shown in the decreased thermostability of sarcosine) and would be further disrupted by betaine (*N*-trimethyl-glycine) that does not promote intramolecular processing. Similarly, the observation that sarcosine can accelerate hASRGL1 cleavage while its isostere  $\beta$ -alanine cannot (Table 4) suggests that the location of the amino group provides important interactions necessary for cleavage.

In our current structure, the complex was obtained by cocrystallizing cp-hASRGL1 with 50 mM glycine. One well-defined glycine molecule was observed close to R196, and a citrate molecule from crystallization buffer was found next to Thr168. In another complex structure by Lavie et al. in which a much higher concentration of glycine was used in crystallization,

they observed the same glycine coordinated to R196 (GLY1) and a second glycine molecule (GLY2) wherein its carboxyl group is positioned 3–4 Å from the amine of GLY1 and 2.6 Å from the T168 hydroxyl group (see PDB entry 4OSX). This observation led them to propose that GLY2 acts as a base to activate T168 and accelerate cleavage.<sup>5</sup> Therefore, the crystal structures suggest that there are two glycine binding pockets with Arg196 coordinating the primary binding site and the one next to Thr168 as a secondary binding site. Given the limited amount of space within the active site, the only molecule larger than glycine that can partially satisfy all the necessary intramolecular contacts is sarcosine. Likewise, glycylamide, although the same size as glycine, cannot form a salt bridge with R196 or provide a carboxyl group for promoting cleavage. Our finding that smaller-than-glycine molecules carbamate and phosphate can also activate hASRGL1 corroborates this hypothesis, suggesting that at high concentrations multiples of these negatively charged molecules can substitute for two glycine molecules.

Finally, given the proximity of GLY1 and GLY2 described in the literature and considering that the conserved R196 residue always forms an electrostatic interaction with small molecule ligands such as glycine, the product L-Asp, or a phosphate from the buffer,<sup>6,19–21</sup> we generated an hASRGL1-R196Q variant to explore the contribution of GLY1 binding to the promotion of cleavage. This variant displayed no activation without glycine, but after incubation with 0.1, 0.25, or 1 M glycine for 48 h, the R196 variant was able to achieve 17, 23, and 34% cleavage, respectively. One interpretation of this data is that binding of GLY2 is predicated on binding of GLY1, as removal of the GLY1 binding site requires very high glycine concentrations to rescue intramolecular processing.

## SUMMARY

In this work, we capitalized on the observation that intramolecular processing of hASRGL1 relieves a torsional strain within the enzyme resulting in a significant increase in thermostability. Implementing a DSF-based assay to measure  $T_M$  values during the hASRGL1 cleavage reaction allowed observation for the first time of distinct molecular species that accumulate, namely, unprocessed homodimer, a half-processed heterotrimer, and fully processed heterotetramer. Kinetic studies revealed that processing occurs in a two-stage process wherein the first cleavage of one of the hASRGL1 subunits has a rate that is markedly faster than the rate of cleavage of the adjacent subunit. The large difference in rates explains why the processing reaction (in the absence of accelerants) proceeds to only ~50% completion. Our studies also illustrate the importance of forming a proper dimer–dimer interface in both maintaining thermal stability and supporting formation of a strained conformation at the scissile peptide bond that allows cleavage to proceed.

The ability to measure hASRGL1 cleavage intermediates by the DSF assay also greatly aided the study of the effect of mutagenesis on conserved active site residues N62, T186, and T219 in their respective roles in catalyzing intramolecular cleavage or substrate hydrolysis. The physical location of these residues relative to the spatially separated substrate and G167 and T168 reaction centers correlates well with their observed rates for both reactions.

## Supplementary Material

Refer to Web version on PubMed Central for supplementary material.

## Acknowledgments

### Funding

This work was supported by National Institutes of Health Grant R01 CA154754, Cancer Prevention and Research Initiative of Texas (CPRIT) Grant RP120314, and Welch Foundation Grant F-1778.

Crystallographic data collection was conducted at the Advanced Light Source (beamline 5.0.3), a Department of Energy (DOE) national user facility. Instrumentation and technical assistance for this work were provided by the Macromolecular Crystallography Facility, with financial support from the College of Natural Sciences, the Office of the Executive Vice President and Provost, and the Institute for Cellular and Molecular Biology at the University of Texas at Austin.

## ABBREVIATIONS

<b>wt</b>	wild-type
<b>hASRGL1</b>	human asparaginase-like protein 1
<b>L-Asn</b>	L-asparagine
<b>L-Asp</b>	L-aspartate
<b>AHA</b>	L-aspartic acid- $\beta$ -hydroxamate
<b>MM</b>	homodimer
<b>MD</b>	heterotrimer
<b>DD</b>	dimer of a heterodimer
<b>Ntn</b>	N-terminal nucleophile
<b>SEC</b>	size exclusion chromatography

## References

1. Cantor JR, Stone EM, Chantranupong L, Georgiou G. The human asparaginase-like protein 1 hASRGL1 is an Ntn hydrolase with beta-aspartyl peptidase activity. *Biochemistry*. 2009; 48:11026–11031. [PubMed: 19839645]
2. Aswad DW, Paranandi MV, Schurter BT. Isoaspartate in peptides and proteins: formation, significance, and analysis. *J Pharm Biomed Anal*. 2000; 21:1129–1136. [PubMed: 10708396]
3. Nomme J, Su Y, Lavie A. Elucidation of the Specific Function of the Conserved Threonine Triad Responsible for Human I-Asparaginase Autocleavage and Substrate Hydrolysis. *J Mol Biol*. 2014; 426:2471–2485. [PubMed: 24768817]
4. Karamitros CS, Konrad M. Bacterial co-expression of the  $\alpha$  and  $\beta$  protomers of human I-asparaginase-3: Achieving essential N-terminal exposure of a catalytically critical threonine located in the  $\beta$ -subunit. *Protein Expression Purif*. 2014; 93:1–10.
5. Su Y, Karamitros CS, Nomme J, McSorley T, Konrad M, Lavie A. Free glycine accelerates the autoproteolytic activation of human asparaginase. *Chem Biol*. 2013; 20:533–540. [PubMed: 23601642]
6. Li W, Cantor JR, Yogesha SD, Yang S, Chantranupong L, Liu JQ, Agnello G, Georgiou G, Stone EM, Zhang Y. Uncoupling Intramolecular Processing and Substrate Hydrolysis in the N-Terminal

- Nucleophile Hydrolase hASRGL1 by Circular Permutation. *ACS Chem Biol.* 2012; 7:1840–1847. [PubMed: 22891768]
7. Niesen FH, Berglund H, Vedadi M. The use of differential scanning fluorimetry to detect ligand interactions that promote protein stability. *Nat Protoc.* 2007; 2:2212–2221. [PubMed: 17853878]
  8. Otwinowski Z, Minor W. Processing of X-ray Diffraction Data Collected in Oscillation Mode. *Methods Enzymol.* 1997; 276:307–326.
  9. Adams PD, Grosse-Kunstleve RW, Hung LW, Ioerger TR, McCoy AJ, Moriarty NW, Read RJ, Sacchettini JC, Sauter NK, Terwilliger TC. PHENIX: building new software for automated crystallographic structure determination. *Acta Crystallogr, Sect D: Biol Crystallogr.* 2002; 58:1948–1954. [PubMed: 12393927]
  10. Emsley P, Cowtan K. Coot: model-building tools for molecular graphics. *Acta Crystallogr, Sect D: Biol Crystallogr.* 2004; 60:2126–2132. [PubMed: 15572765]
  11. Brunger AT. Free R value: a novel statistical quantity for assessing the accuracy of crystal structures. *Nature.* 1992; 355:472–475. [PubMed: 18481394]
  12. Laskowski RA, Macarthur MW, Moss DS, Thornton JM. Procheck - a Program to Check the Stereochemical Quality of Protein Structures. *J Appl Crystallogr.* 1993; 26:283–291.
  13. Chen VB, Arendall WB 3rd, Headd JJ, Keedy DA, Immormino RM, Kapral GJ, Murray LW, Richardson JS, Richardson DC. MolProbity: all-atom structure validation for macromolecular crystallography. *Acta Crystallogr, Sect D: Biol Crystallogr.* 2010; 66:12–21. [PubMed: 20057044]
  14. Wang Y, Guo HC. Two-step dimerization for autoproteolysis to activate glycosylasparaginase. *J Biol Chem.* 2003; 278:3210–3219. [PubMed: 12433919]
  15. Wang Y, Guo HC. Crystallographic snapshot of glycosylasparaginase precursor poised for autoprocessing. *J Mol Biol.* 2010; 403:120–130. [PubMed: 20800597]
  16. Buller AR, Labonte JW, Freeman MF, Wright NT, Schildbach JF, Townsend CA. Autoproteolytic activation of ThnT results in structural reorganization necessary for substrate binding and catalysis. *J Mol Biol.* 2012; 422:508–518. [PubMed: 22706025]
  17. Frohwein YZ, Friedman M, Reizer J, Grossowicz N. Sensitive and rapid assay for L-asparaginase. *Nat New Biol.* 1971; 230:158–159. [PubMed: 5279475]
  18. Harris, DC., editor. *Quantitative Chemical Analysis.* 6. W. H. Freeman; New York: 2002.
  19. Qian XF, Guan CD, Guo HC. A dual role for an aspartic acid in glycosylasparaginase autoproteolysis. *Structure.* 2003; 11:997–1003. [PubMed: 12906830]
  20. Michalska K, Brzezinski K, Jaskolski M. Crystal structure of isoaspartyl aminopeptidase in complex with L-aspartate. *J Biol Chem.* 2005; 280:28484–28491. [PubMed: 15946951]
  21. Prahl A, Pazgier M, Hejazi M, Lockau W, Lubkowski J. Structure of the isoaspartyl peptidase with L-asparaginase activity from *Escherichia coli*. *Acta Crystallogr, Sect D: Biol Crystallogr.* 2004; 60:1173–1176. [PubMed: 15159592]
  22. Nomme J, Su Y, Konrad M, Lavie A. Structures of apo and product-bound human L-asparaginase: insights into the mechanism of autoproteolysis and substrate hydrolysis. *Biochemistry.* 2012; 51:6816–6826. [PubMed: 22861376]

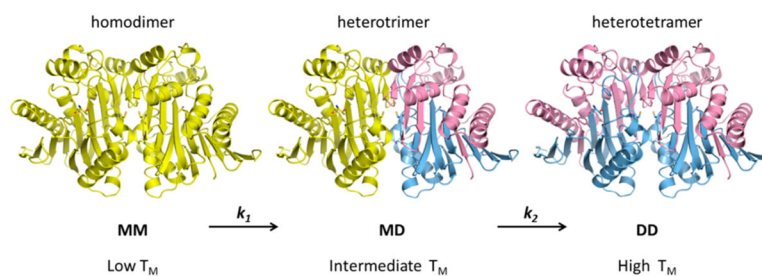


**Figure 1.** Schematic model of hASRGL1 intramolecular processing. MM represents the unprocessed homodimer (unprocessed monomer, yellow). MD represents the intermediate species of a heterotrimer with one processed monomer with the  $\alpha$  subunit (light pink) and  $\beta$  subunit (light blue) split from a monomer. DD represents fully processed hASRGL1 of a heterotetramer with a dimer of a heterodimer.  $k_1$  is the rate of first-step hASRGL1 processing, and  $k_2$  is the second rate of processing.

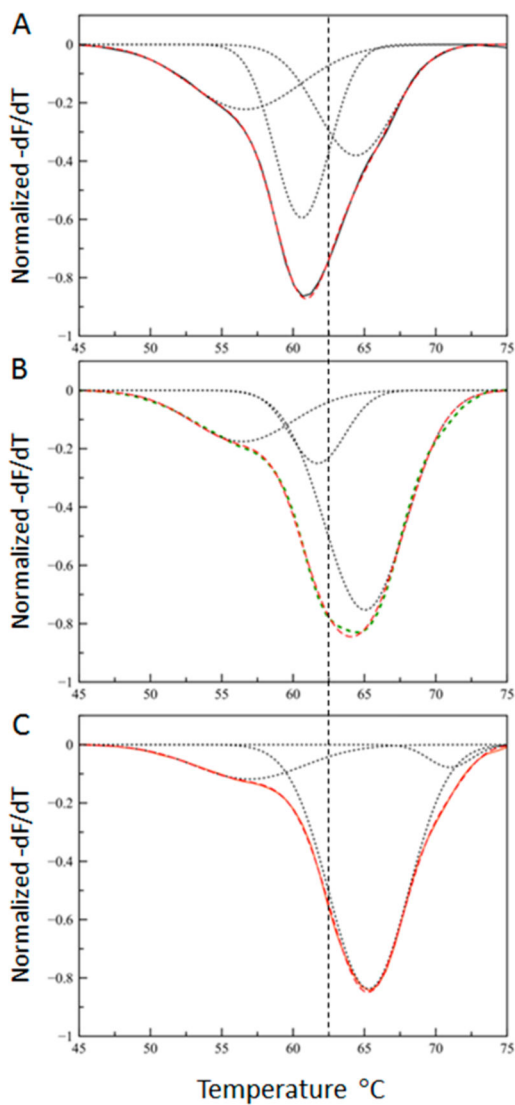


**Figure 2.**

DSF analysis of wt-hASRGL1 intramolecular processing. Thermal denaturation profile of wt-hASRGL1 during processing fitted by summation of Gaussian equations (dashed red line). (A) At time zero, the  $dF/dT$  area is well fitted to three Gaussian curves with a main peak at 61 °C and two shoulders at 56 and 65 °C. (B) At the 8 h time point, the 65 °C peak is now the major species. (C) By 48 h, the 61 °C peak is gone with the appearance of a small new shoulder at ~71 °C.



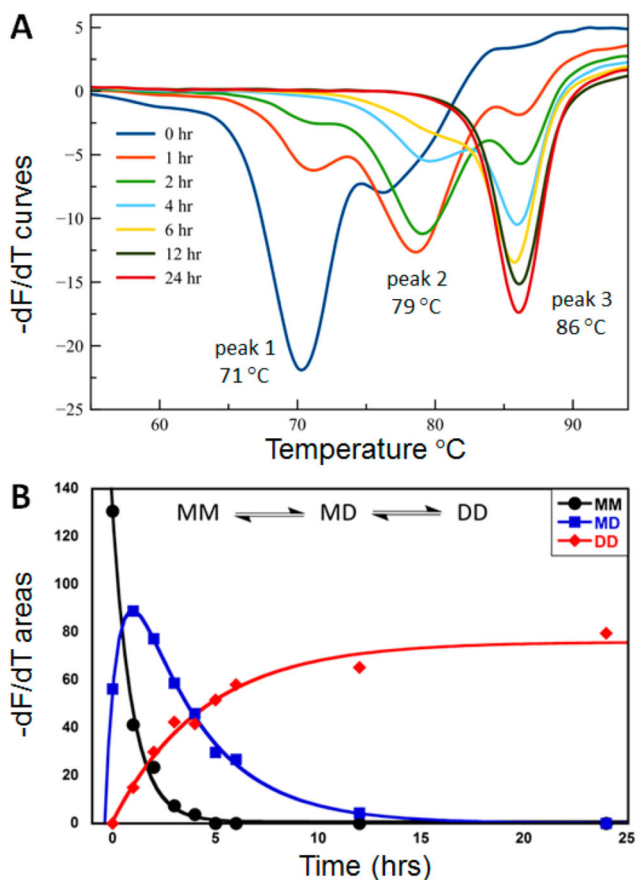


**Figure 3.** Time course of intramolecular processing in the presence of glycine. (A) Protein melting profile of hASRGL1 processing in the presence of 1 M glycine. Each colored line represents one protein melting curve at the indicated time point. (B) Resulting areas under the  $-dF/dT$  curves of panel A were fit to a  $MM \rightarrow MD \rightarrow DD$  kinetic model, wherein MM is the unprocessed homodimer, MD is the half-processed heterotrimer, and DD is the fully processed heterotetramer.

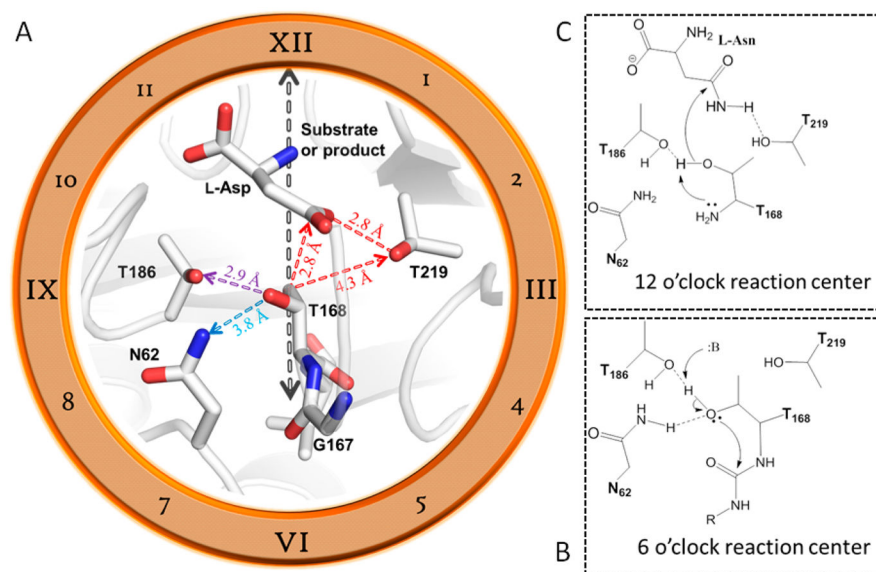


**Figure 4.**

Active site configuration of hASRGL1. (A) Clock diagram of hASRGL1 reaction centers and distances derived from superimposition of currently known structures of hASRGL1 (the structure reported in this paper and PDB entries 4OSX and 4PVR<sup>5,22</sup>). (B) Hydrogen bonds from N62 and T186 (8 and 10 o'clock, respectively) to the hydroxyl group of T168 facilitate a nucleophilic attack on the G167-T168 peptide bond (6 o'clock) to cleave and activate hASRGL1. (C) Substrate binds the active site at 12 o'clock where the  $\gamma$ -hydroxyl of T186 assists in deprotonation of the T168  $\gamma$ -hydroxyl group during nucleophilic attack on the substrate amide group. The T219  $\gamma$ -hydroxyl (2 o'clock) aids in stabilizing the Michaelis complex and the leaving group.

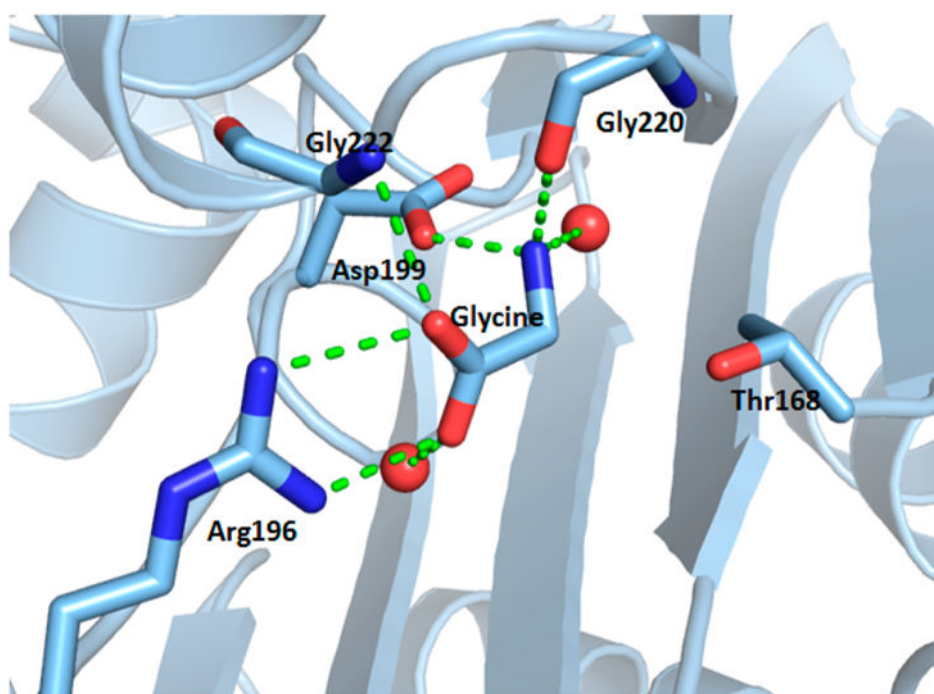


**Figure 5.** Cocrystal structure of glycine-bound cp-hASRGL1. Glycine binding to hASRGL1 is stabilized by a salt bridge from R196 and by hydrogen bond interactions [green dashed line (from D199, G220, G222, and two water molecules)].

Table 1

## Crystallographic Data and Refinement Statistics for cp-hASRGL1

Crystallographic Statistics	
source	ALS 5.0.3
wavelength (Å)	0.98
resolution (Å)	50–2.52 (2.52–2.56) <sup>d</sup>
space group	<i>P</i> 212121
unit cell ( <i>a</i> , <i>b</i> , <i>c</i> ) (Å)	104.33, 111.10, 122.50
data cutoff	<i>F</i> > 0
mol. per asymmetric unit	4
no. of unique reflections	49219
redundancy	4.5 (4.4)
completeness (%)	99.9 (100.0)
<i>I</i> /σ( <i>I</i> )	11.9 (3.05)
<i>R</i> <sub>sym</sub> (%)	12.8 (43.3)
<i>R</i> <sub>pim</sub> (%)	6.8 (23.5)
CC <sub>1/2</sub>	0.932
Refinement Statistics	
resolution limit (Å)	39.74–2.51
no. of reflections (test)	46618 (3195)
data cutoff	0
<i>R</i> <sub>work</sub> , <i>R</i> <sub>free</sub> (%) <sup>b</sup>	20.4, 23.3
no. of atoms	8838
protein	8658
water	74
Na	4
DTT <sup>c</sup>	16
glycine	20
citrate	26
BME <sup>d</sup>	40
<i>B</i> factor (Å <sup>2</sup> )	28.61
protein	28.47
water	19.85
Na	31.46
DTT <sup>c</sup>	55.74
glycine	25.46
citrate	60.19
BME <sup>d</sup>	52.99
root-mean-square deviation	
bond lengths (Å)	0.015
bond angles (deg)	1.684

---

**Crystallographic Statistics**

MolProbity score <sup>e</sup>	1.65 (99th percentile)
poor rotamer (%)	1.57
Clashscore	6.21 (99th percentile)
Ramachandran outliers (%)	0.00
Ramachandran favored (%)	97.09

---

<sup>a</sup>Data for the highest-resolution shell are given in parentheses.

<sup>b</sup> $R_{\text{free}}$  calculated with 5% of the data randomly omitted from refinement.

<sup>c</sup>Dithiothreitol.

<sup>d</sup> $\beta$ -Mercaptoethanol.

<sup>e</sup>MolProbity score combines the Clashscore, rotamer, and Ramachandran evaluation into a single score, normalized to be on the same scale as X-ray.

Table 2

Intramolecular Processing and Rates for hASRGL1 and Its Variants

variant	activator	MM → MD $k_1$ ( $\text{h}^{-1}$ )	x-fold change in $k_1$	MD → DD $k_2$ ( $\text{h}^{-1}$ )	x-fold change in $k_2$
wt activation					
hASRGL1	–	0.034	–	0.002	–
hASRGL1	Gly	1	29	0.40	200
hASRGL1	sarcosine	0.11	3	0.08	40
hASRGL1	(NH <sub>4</sub> ) <sub>3</sub> PO <sub>4</sub>	0.06	2	0.04	20
dimer-dimer interface variants					
hASRGL1-C202A <sup>a</sup>	–	nd	–	nd	–
hASRGL1-C202S <sup>a</sup>	–	nd	–	nd	–
hASRGL1-C202A	Gly	0.80	-1.3	0.30	-1
hASRGL1-C202S	Gly	0.60	-1.7	0.20	-2
hASRGL1-C202V	Gly	1.10	1	0.60	1.5
active site variants					
hASRGL1-T219S	Gly	0.14	-7	0.11	-4
hASRGL1-T219A	Gly	0.15	-7	0.07	-6
hASRGL1-N62A	Gly	0.30	-3	nd	–
hASRGL1-N62D	Gly	0.36	-3	0.06	-7
hASRGL1-T186S	Gly	0.44	-2	0.32	-1
hASRGL1-T186A	Gly	0.06	-17	0.02	-20
% cleavage					
hASRGL1-T219S <sup>a</sup>				50	
hASRGL1-T219A <sup>a</sup>				50	
hASRGL1-N62A <sup>a</sup>				0	
hASRGL1-N62D <sup>a</sup>				5–10	
hASRGL1-T186S <sup>a</sup>				50	
hASRGL1-T186A <sup>a</sup>				0	

<sup>a</sup> Abbreviations: nd, none detected; asterisk, after incubation for 48 h; Gly, glycine; (NH<sub>4</sub>)<sub>3</sub>PO<sub>4</sub>, ammonium phosphate.

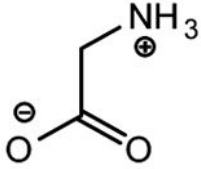
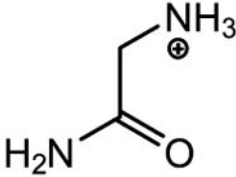
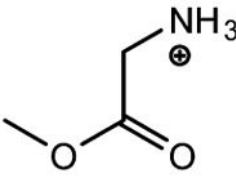
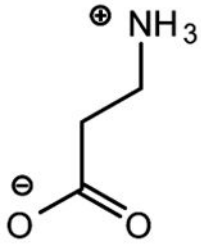
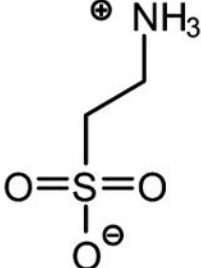
**Table 3**

## Kinetic Parameters of hASRGL1 Variant Hydrolysis of AHA

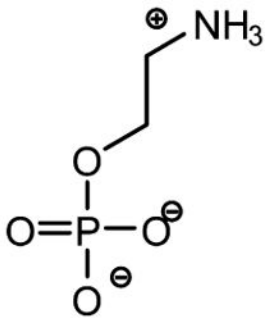
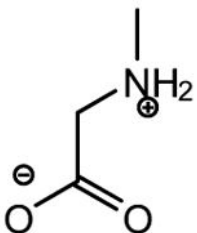
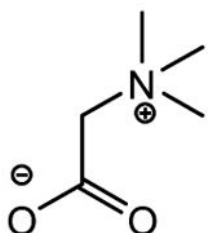
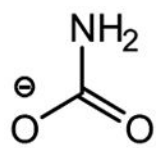
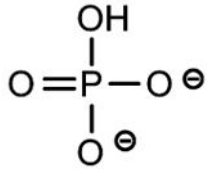
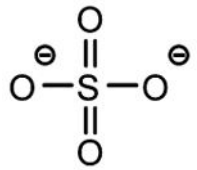
variant	$k_{\text{cat}}$ ( $\text{s}^{-1}$ )	x-fold change in $k_{\text{cat}}$ (wt vs variant)	$K_M$ (mM)	$k_{\text{cat}}/K_M$ ( $\text{s}^{-1} \text{mM}^{-1}$ )	x-fold change in $k_{\text{cat}}/K_M$ (wt vs variant)	
cp-hASRGL1	$10.5 \pm 0.3$	1	$0.2 \pm 0.01$	$60 \pm 4$	1	1
cp-hASRGL1-T219S	$0.4 \pm 0.01$	-26	$0.3 \pm 0.01$	$1.4 \pm 0.1$		-40
cp-hASRGL1-T219A	$0.1 \pm 0.02$	-100	$1.3 \pm 0.7$	$0.1 \pm 0.04$		-600
cp-hASRGL1-N62A	$1.3 \pm 0.2$	-8	$0.3 \pm 0.1$	$4.5 \pm 2.0$		-13
cp-hASRGL1-N62D	$1.8 \pm 0.1$	-6	$0.2 \pm 0.1$	$9.0 \pm 2.0$		-7
cp-hASRGL1-T186S	$5.8 \pm 0.8$	-2	$1.8 \pm 0.4$	$3.3 \pm 0.8$		-18
cp-hASRGL1-T186A	$0.02 \pm 0.001$	-530	$0.6 \pm 0.05$	$0.03 \pm 0.003$		-2000

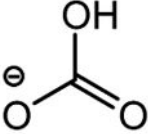
**Table 4**

Molecules Screened for Promoting hASRGL1 Intramolecular Processing

Molecule	Structure	Activator
Glycine		+++
Glycinamide		-
Glycine-methyl-ester		-
$\beta$ -alanine		-
Taurine		-



Molecule	Structure	Activator
o-phosphoryl-ethanolamine		-
Sarcosine		+
Betaine		-
Carbamate		+
Phosphate		+
Sulfate		-

Molecule	Structure	Activator
Bicarbonate	 <p>The image shows the chemical structure of the bicarbonate ion (HCO<sub>3</sub><sup>-</sup>). It consists of a central carbon atom bonded to three oxygen atoms and one hydrogen atom. One oxygen atom is double-bonded to the carbon, and the other two are single-bonded. One of the single-bonded oxygen atoms has a negative charge (represented by a minus sign in a circle). The hydrogen atom is bonded to the carbon and one of the single-bonded oxygen atoms.</p>	-

Author Manuscript

Author Manuscript

Author Manuscript

Author Manuscript